Continuum Mech. Thermodyn. (2002) 14: 437–457
Digital Object Identifier (DOI) 10.1007/s001610200083

Original Article

A mechanism of transformational plasticity

G. Puglisi[1], **L. Truskinovsky**[2]

[1] Dipartimento di Ingegneria Civile e Ambientale, Politecnico di Bari, 70124, Bari, Italy
[2] Department of Aerospace Engineering and Mechanics, University of Minnesota, MN 55455, USA

Received December 28, 2001 / Published online June 4, 2002 –
Communicated by Kolumban Hutter, Darmstadt

In order to understand the phenomenon of reversible plasticity exhibited by shape memory alloys and other smart materials, we study an elementary prototypical model. Building on an original idea of Müller and Villaggio [17], we consider an inhomogeneous ensemble of bi-stable elements connected in series and loaded in a soft device. To interpret the fine structure of the hysteresis loops observed experimentally, we assume that the dynamics is maximally dissipative and investigate different evolutionary strategies for a "driven" system with external force changing quasi-statically. Our main result is that the inhomogeneity of the elastic properties leads to a distinctive hardening with serrations of a Portevin-Le Chatelier type and produces a realistic memory structure characterized by the "congruency" and "return point memory" properties.

Introduction

In recent years the behavior of smart materials has been repeatedly addressed via lattice models with bi-stable elements (e.g. [17],[16],[10],[28],[27],[2],[3]). What makes discrete models particularly attractive, is their ability to generate complex energy landscapes with multiple local minima. The presence in these models of a large number of metastable states creates a potential for trapping, hysteresis, and history dependence in the constitutive structure. Moreover, internal instabilities provide a mechanism for the energy escape into high frequency modes even in the quasistatic processes.

The simplest case of a one-dimensional lattice with bi-stable elements is relevant primarily in the context of transformational plasticity as observed for instance in shape memory alloys. The one dimensional model may be used as a description of both tension tests (longitudinal deformation of a chain of particles) and shear tests (transversal deformation of a "deck of cards"). Although the modeling of metal plasticity may call for multi-stability of the elastic elements [11], while description of fracture may require one of the wells to be placed at infinity [36], the case of a chain with bi-stable springs may be considered an important starting point for the qualitative analysis of all these seemingly diverse phenomena.

In the present paper we extend the results of [26] and [27], where we studied bi-stable systems with identical elements, to the case when the elemental parameters are allowed to fluctuate according to a prescribed probability distribution. The assumed inhomogeneity results from the presence in the real crystals of dislocations, grain boundaries, and other defects. Since different elements in the inhomogeneous system may transform at different stresses, the effective "material" exhibits characteristic hardening, in agreement with what is observed in experiments ([9],[21],[23]). It should be noted that the so defined inhomogeneity is not

Dedicated to Ingo Müller on the occasion of his 65th birthday

the only mechanism of hardening in real crystals: numerous other contributions range from latent heat and defects interaction to viscoelasticity and dynamics.

As in [27] we assume that the system is overdamped and study its evolution under quasi-static loading. Our previous analysis of the equilibrium problem in the homogeneous case revealed the existence of a multiplicity of metastable configurations whose variety increases even further when the chain becomes inhomogeneous. As we show, the evolution of such a system goes through a sequence of abrupt transitions between neighboring local minima. The overall behavior can be described as "stick-slip", with purely elastic deformation in the "stick" phase and with "plastic" transitions between elastic branches in the "slip" phase. We remark that in the slow time scale of the external loading the fast flip-over phenomena can be considered instantaneous. Also, since in the quasi-static setting the elastic stages are conservative, the dissipation in our model is associated exclusively with the switching events. To avoid the detailed discussion of the fast motions accompanying internal loss of stability (see, for instance, [32],[2],[3],[30],[31],[6]) we assume that the relaxation proceeds along the path of the steepest descent. In addition we suppose that, due to the presence of thermal and mechanical fluctuations, the system is able to climb energy barriers of small, but finite height.

With these simplifying assumptions at hand, we demonstrate that loaded periodically our inhomogeneous bi-stable chain exhibits a realistic hysteresis, with hardening, elastic unloading, Bauschinger effect, return point memory, and congruency of the inner loops, all well documented experimentally ([7],[13],[15],[22],[35]). We show that an alternate sequence of slow "elastic" and fast "plastic" steps leads to the distinctive serrations on the stress-strain curves typical of the Portevin-Le Chatelier effect and observed experimentally for both transformational and regular plasticity (e.g.[4],[8],[37]). We demonstrate that in our model the fraction of external work irreversibly dissipated into heat during the transformation process is not fixed, but depends on the loading history and the extent of the inhomogeneity. To make a link with a considerable body of literature on formal modeling of rate independent hysteresis, we construct an equivalent Preisach model and discuss the relation between the two approaches.

The structure of the paper is as follows. In Sect. 1 we formulate the model and introduce the parameters that describe the inhomogeneity. Equilibrium and stability properties of the model are studied in Sect. 2. We then explore in Sect. 3 the structure of the non-equilibrium energy landscape and show that the "minimal barrier crossing" strategy requires successive transformations inside individual springs. In Sect. 4 we discuss the stick-slip transformation mechanism associated with the crossing of fixed-size barriers and subsequent steepest descent into the "nearest" energy wells. In Sect. 5 we look into the fine structure of the hysteresis and study the configuration of the internal loops. The continuum limit and the equivalent Preisach model are discussed in Sect. 6. Two Appendixes contain technical proofs.

1 The model

Consider a chain formed by n bi-stable elastic springs connected in series. The chain is placed in a soft device and is loaded by a given force $\bar{\sigma}$. To find the equilibrium configurations of this mechanical system we need to minimize its potential energy

$$G = \sum_{i=1}^{n} a(\varphi_i(\varepsilon_i) - \bar{\sigma}\varepsilon_i). \tag{1.1}$$

Here $a = L/n$ is the reference length, $a\varphi_i(\varepsilon_i)$ is the elastic energy of the i-th spring, and ε_i is the corresponding strain defined as the elongation divided by the reference length. We are interested in the case when the energies φ_i are non-convex so that the corresponding force-strain relation $\sigma_i = \varphi_i'(\varepsilon_i)$ is non-monotone. For purely technical reasons, we will be mostly dealing with tri-parabolic energies of the type

$$\varphi(\varepsilon) := \begin{cases} \dfrac{1}{2}(\varepsilon+1)^2 + \sigma_M\varepsilon, & \varepsilon < -t, \\ \dfrac{1}{2}\left(\dfrac{t-1}{t}\varepsilon^2 + 1 - t\right) + \sigma_M\varepsilon, & -t \le \varepsilon \le t, \\ \dfrac{1}{2}(\varepsilon-1)^2 + \sigma_M\varepsilon, & t < \varepsilon. \end{cases} \tag{1.2}$$

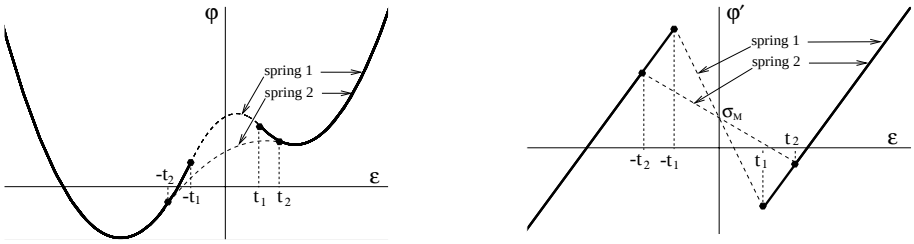

Fig. 1. Energy-strain and force-strain relations for the springs (1.2) with $t = t_1 = 0.4$ and $t = t_2 = 0.7$

The function (1.2) is convex on two disjoint intervals (energy wells) separated by the spinodal region where it is concave. The energy depends on two parameters: σ_M prescribing the phase equilibrium (or Maxwell) force and $t \in (0, 1)$ controlling the size of the spinodal region; we have tacitly assumed that the energy wells at $\bar{\sigma} = \sigma_M$ are located at $\varepsilon = \pm 1$. The tri-linear model (1.2), while preserving most of the qualitative properties of the more general double-well models (see the comparison in [26]), has the advantage of furnishing most of the results in an explicit form.

In the previous paper [27] we considered an over-symmetric case when all springs are identical and $\varphi_i = \varphi$, $i = 1, \ldots, n$. As a result the system was degenerate and some important physical phenomena were concealed by an excessive symmetry. In the present paper we assume that the parameters of the springs may vary along the chain. To make the analysis more transparent we make an additional simplifying assumption that only the size of the spinodal region t_i fluctuates while the Maxwell force remains constant for all springs, $\sigma_{M_i} = \sigma_M$, $i = 1, \ldots, n$. Essentially we will be dealing with an ensemble of bi-stable elements whose two (identical) energy wells are separated by a variable barrier (see Fig. 1).

To characterize the statistical properties of the ensemble, we introduce a probability density $p = p(t)$, satisfying $\int_0^1 p(t)\,dt = 1$. Although the actual spatial distribution of springs is irrelevant for the behavior of the system at the "macro-scale", in order to be able to illustrate the evolving phase distribution we assume a particular dispersion of spring properties. We define a function $\hat{t}(x)$ which assigns to a generic point with coordinate x a specific value of the parameter t; without loss of generality one may assume that $\hat{t}\,'(x) > 0$. Since the inverse function $\hat{x} := \hat{t}^{-1}$ satisfies $\hat{x}(\bar{t})/L = \int_0^t p(t)\,dt$, the continuous spatial distribution $\hat{t}(x)$ is easily recovered from $p = p(t)$. The discrete distribution is then $t_i = \hat{t}(Li/n)$, $i = 0, \ldots, n-1$. For convenience we will be calling the springs with high (low) value of t as weak (strong). According to our assumption the last spring is the "weakest", while the first one is the "strongest". For numerical computations we use Gaussian distributions $p(t) = \alpha e^{-\beta(t-t_0)^2}$ with parameters β and $t_0 \in (0, 1)$ given and $\alpha = \alpha(\beta, t_0)$ adjusted to satisfy the normalization condition. Two sample distributions of this kind are illustrated in Fig. 2; the homogeneous chain, studied in [27], corresponds to the case when $p = p(t)$ is a Dirac delta function.

2 Equilibrium and stability

The equilibrium equations in our problem establish the continuity of the force inside the chain

$$\varphi_i'(\varepsilon_i) = \bar{\sigma}, \quad i = 1, \ldots, n. \tag{2.1}$$

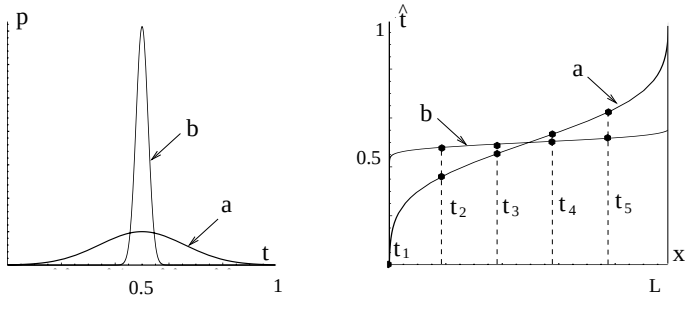

Fig. 2. Gaussian distributions $p = p(t)$ and $\hat{t}(x)$ for a chain with $n = 5$, $t_0 = 1/2$ and $\beta = 20$ (a) or $\beta = 1000$ (b)

Introduce $\tilde{\sigma} := \bar{\sigma} - \sigma_M$ and consider $\tilde{\sigma} \in (t_i - 1, 1 - t_i)$. Then for each spring the equilibrium equation (2.1) have three different solutions, which we distinguish as phases I, II, and III:

$$\varepsilon_i^I(\tilde{\sigma}) := \tilde{\sigma} - 1, \quad \varepsilon_i^{II}(\tilde{\sigma}) := \frac{t_i}{t_i - 1}\tilde{\sigma}, \quad \varepsilon_i^{III}(\tilde{\sigma}) := \tilde{\sigma} + 1. \tag{2.2}$$

Outside the interval $(t_i - 1, 1 - t_i)$ the solution is unique: specifically, if $\tilde{\sigma} < t_i - 1$ then $\varepsilon_i = \varepsilon_i^I(\tilde{\sigma})$, and if $\tilde{\sigma} > 1 - t_i$, $\varepsilon_i = \varepsilon_i^{III}(\tilde{\sigma})$. For a given $\bar{\sigma}$ the equilibrium configuration of the chain can be characterized by a $3 \times n$ phase matrix χ_i^α, with $\chi_i^\alpha = 1$ if the i-th spring is in phase α, and $\chi_i^\alpha = 0$ otherwise ($\alpha = I, II, III$, $i = 1, \dots, n$). The state of the chain can be also described by the following three sets $\mathcal{I}^\alpha = \{i \in \{1, \dots, n\} : \chi_i^\alpha = 1\}$. A less detailed characterization of the equilibrium configuration is provided by the "phase fractions" k, l, m, equal to the numbers of springs in phase I, II, and III, respectively. One can see that $k = \sum_{i=1}^n \chi_i^I$, $l = \sum_{i=1}^n \chi_i^{II}$, and $m = \sum_{i=1}^n \chi_i^{III}$, with $k + l + m = n$.

Given the phase matrix χ_i^α, the overall strain $\bar{\varepsilon}$, the total elastic energy $\bar{\Phi}$, and the potential energy $\bar{G}$ of an equilibrium configuration can be written as

$$\begin{aligned}
\bar{\varepsilon} &:= \frac{1}{n}\sum_i \varepsilon_i = \frac{1}{n}\sum_{i,\alpha} \chi_i^\alpha \varepsilon_i^\alpha, \\
\bar{\Phi} &:= a\sum_i \varphi_i(\varepsilon_i) = a\sum_{i,\alpha} \chi_i^\alpha \varphi_i(\varepsilon_i^\alpha), \\
\bar{G} &:= a\sum_i (\varphi_i(\varepsilon_i) - \bar{\sigma}\varepsilon_i) = a\sum_{i,\alpha} \chi_i^\alpha (\varphi_i(\varepsilon_i^\alpha) - \bar{\sigma}\varepsilon_i^\alpha).
\end{aligned} \tag{2.3}$$

Using (1.2) and (2.2) we obtain

$$\begin{aligned}
\bar{\varepsilon} &= \frac{\tilde{\sigma}}{E} + \varepsilon_0, \\
\frac{\bar{\Phi}}{L} &= \frac{\tilde{\sigma}^2}{2E} + \sigma_M \bar{\varepsilon}(\tilde{\sigma}) + \frac{1}{2n}\sum_{i=1}^n \chi_i^{II}(1 - t_i), \\
\frac{\bar{G}}{L} &= -\frac{\tilde{\sigma}^2}{2E} - \tilde{\sigma}\varepsilon_0 + \frac{1}{2n}\sum_{i=1}^n \chi_i^{II}(1 - t_i).
\end{aligned} \tag{2.4}$$

Here $\varepsilon_0 = (m - k)/n$ characterizes the reference strain at the Maxwell force for the corresponding branch of equilibria, while

$$E := \frac{n}{\sum_{i=1}^n 1/E_i} \tag{2.5}$$

plays the role of "effective" elastic modulus; the parameters E_i describe the elasticities of the individual elements, with $E_i = 1$ in phases I or III and $E_i = (t_i - 1)/t_i$ in phase II. According to (1.2) the equilibrium solutions are defined for $\tilde{\sigma} \in (s_{\min}, s_{\max})$, with $s_{\min} := \max_{i \in \mathcal{I}^{II} \cup \mathcal{I}^{III}}(t_i - 1)$ and $s_{\max} := \min_{i \in \mathcal{I}^I \cup \mathcal{I}^{II}}(1 - t_i)$.

The analysis of the local stability for the equilibria (2.1) is straightforward. Thus, a solution is metastable (corresponds to a local minimum of the energy) if the Hessian matrix

$$\begin{Vmatrix} E_1 & 0 & \dots & 0 \\ 0 & E_2 & \dots & 0 \\ \dots & \dots & \dots & \dots \\ 0 & 0 & \dots & E_n \end{Vmatrix}$$

is positive definite. This means all $E_i > 0$ and we can conclude that the metastable configurations can contain elements in phases I and III only. Consequently $\chi_i^{II} = 0$ and the metastable states can be completely described by the vector χ_i^I. Since the metastable branches with the same value of k have the same reference strain

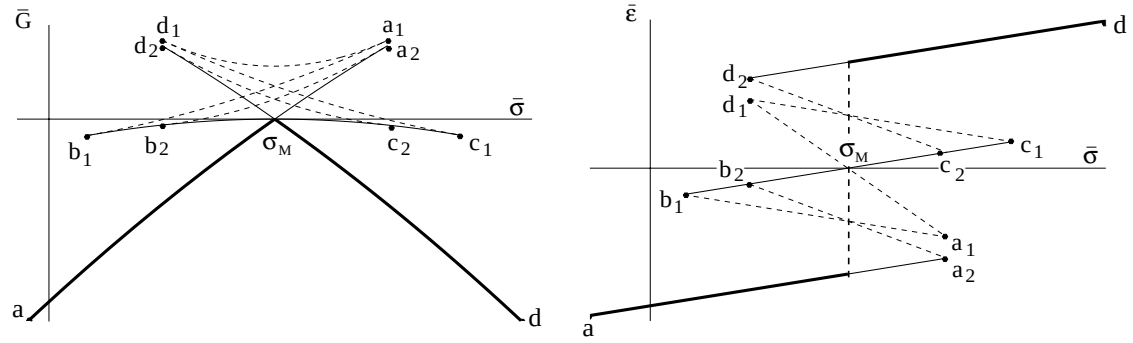

$aa_2=\begin{bmatrix}1&1\\0&0\\0&0\end{bmatrix}$ $a_2b_2=\begin{bmatrix}1&0\\0&1\\0&0\end{bmatrix}$ $a_1b_1=\begin{bmatrix}0&1\\1&0\\0&0\end{bmatrix}$ $b_1c_2=\begin{bmatrix}0&1\\0&0\\1&0\end{bmatrix}$ $a_1d_1=\begin{bmatrix}0&0\\1&1\\0&0\end{bmatrix}$ $b_2c_1=\begin{bmatrix}1&0\\0&0\\0&1\end{bmatrix}$ $c_1d_1=\begin{bmatrix}0&0\\1&0\\0&1\end{bmatrix}$ $c_2d_2=\begin{bmatrix}0&0\\0&1\\1&0\end{bmatrix}$ $d_2d=\begin{bmatrix}0&0\\0&0\\1&1\end{bmatrix}$

Fig. 3. Equilibrium potential energy and strain for a chain with $n = 2$. Each equilibrium branch is labeled by its phase matrix χ_i^α presented at the bottom of the figure. *Bold lines* indicate global minima of the potential energy, *solid lines* – local minima, and *dashed lines* – unstable equilibrium configurations. Here $t_1 = 0.75$, $t_2 = 0.85$, and $\sigma_M = 0.3$

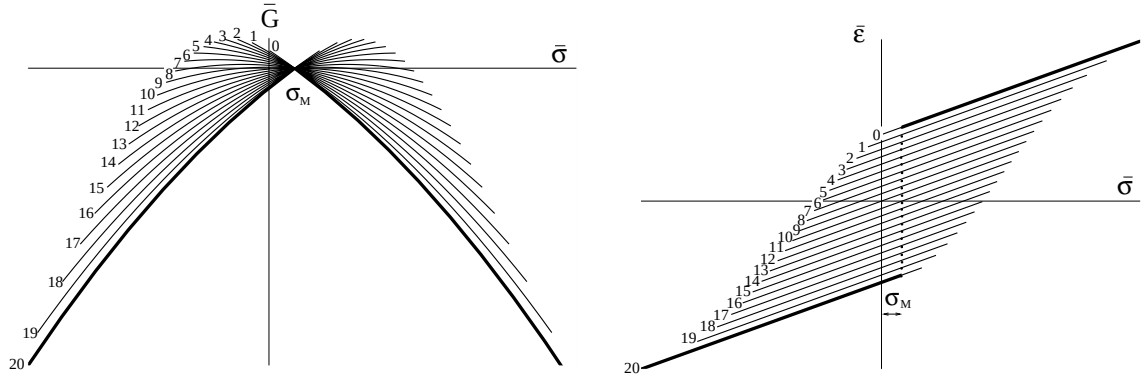

Fig. 4. Potential energy and strain for the metastable configurations of a chain with $n = 20$. Bold line represent the global minimum of the energy. Here $\beta = 5$, $t_0 = 0.5$, and $\sigma_M = 0.1$

ε_0, they are superimposed and can be distinguished only through their respective limits of stability. As an illustration, we present in Fig. 3 a complete set of equilibrium branches for the simplest inhomogeneous chain with two springs, $n = 2$.

The metastable branches (only) for a chain with $n = 20$ springs are shown in Fig. 4. We notice that the global minimum of the energy is represented by the homogeneous configurations with either $k = n$, when $\tilde{\sigma} < 0$, or $k = 0$, when $\tilde{\sigma} > 0$; the transition between these branches occurs exactly at the Maxwell force $\tilde{\sigma} = 0$.

3 Energy landscape

In "wiggly" energy landscapes the evolution of a system is regulated by its capacity to overcome energy barriers. To analyze the available strategies and the associated hysteresis patterns, one needs to know the detailed topography of the energy surface outside the critical points. We begin with the simplest case of a chain with only two springs and then pass to the general case of an arbitrary number of springs.

3.1 Chain with two springs

Consider the case $n = 2$ with $t_2 > t_1$, meaning that the first spring is "stronger" than the second. For the purpose of comparison with the homogeneous case [27] we describe the state of the chain by the same two order parameters $\bar{\varepsilon}$ and ξ, such that $\varepsilon_1 = \bar{\varepsilon} + \xi$ and $\varepsilon_2 = \bar{\varepsilon} - \xi$. In Fig. 5 we illustrate the landscape of the total energy $G = \varphi_1(\bar{\varepsilon} - \xi) + \varphi_2(\bar{\varepsilon} + \xi) - 2\bar{\sigma}\bar{\varepsilon}$ in the plane of the order parameters at two different values of the applied force $\tilde{\sigma}$. The case of Maxwell force $\tilde{\sigma} = 0$ is shown in Fig. 5c, while a generic case $\tilde{\sigma} \in (0, 1 - t_2)$ is shown in Fig. 5.

For $\tilde{\sigma} \in (t_2 - 1, 1 - t_2)$ we observe four different local minima: the single phase configuration I (m_d), the single phase configuration III (m_a), and two two-phase configurations - with the first spring in phase I and the second in phase III (m_b), and the symmetric one with these two springs interchanged (m_c). The analysis of the figures suggests that the minimum energy barrier leading away from the basin of the minimum m_d corresponds to the saddle s_c, with the "weakest" of the two springs, $i = 2$, in the spinodal state $\varepsilon_2 = \varepsilon^{II}(\bar{\sigma})$ and with the "strongest" spring, $i = 1$, remaining in phase I. Using (2.2) one can show that the critical points m_d, s_c, and m_b are connected by the straight line

$$\xi = -\bar{\varepsilon} - 1 + \tilde{\sigma}. \tag{3.1}$$

Observe that along this path $\varphi'(\varepsilon_1) = \varepsilon_1 + 1 + \sigma_M = \bar{\sigma}$ meaning that the first spring stays in equilibrium even as the second spring changes phase along a nonequilibrium path. Notice also that this trajectory describes the steepest descent from the saddle s_c to the minimum m_b. The energy barrier along this path between the metastable states m_d and m_b is equal to

$$h_2(\tilde{\sigma}) = a\frac{(1 - t_2 - \tilde{\sigma})^2}{2(1 - t_2)}.$$

Here the sub index 2 indicates that the "non-equilibrium" transformation is taking place in the second spring.

Once the system is in m_b it needs to overcome another barrier before it arrives into the global minimum m_a. Following the same logics we obtain that the minimum barrier path goes through the saddle s_b describing the state with the spring $i = 1$ in the spinodal region. The local minimum m_b is connected to the saddle s_b and further to the global minimum m_a by the path

$$\xi = \bar{\varepsilon} - 1 - \tilde{\sigma}. \tag{3.2}$$

Along this path it is the spring $i = 1$ which transforms, while the spring $i = 2$ remains in the equilibrium configuration preset by the equilibrium condition $\varphi_2'(\varepsilon_2) = \bar{\sigma}$. The energy barrier is now equal to

$$h_1(\tilde{\sigma}) = a\frac{(1 - t_1 - \tilde{\sigma})^2}{2(1 - t_1)}.$$

By combining the two paths (3.1) and (3.2) we obtain the energy landscape presented in Fig. 5e,f by the bold lines. One can view this section of the global energy surface as the analog of the Peierls landscape in the theory of dislocations [19]; in our context it describes the discretization induced energy barriers associated with the advancement of the "transformation front" (cf. effective 1D energy landscape in [1]). Since $t_2 > t_1$ we obtain that $h_1(\tilde{\sigma}) > h_2(\tilde{\sigma})$, which means that, contrary to the case of a homogeneous chain [27], the "minimal" barriers for the successive switching events inside the individual springs increase as the transformation advances. As it will be clear from the next section, this unevenness of the "Peierls barriers" has important implications for the hardening behavior of the chain.

3.2 General case

The results obtained for $n = 2$ can be extended to the general case of a chain with an arbitrary number n of springs. Consider a generic metastable state A with $\hat{k} \neq 0$ springs in phase I and $n - \hat{k}$ springs in phase III. To simplify the analysis we rearrange the indexes so that the first $\hat{k}$ springs are in phase I and the remaining $n - \hat{k}$ springs are in phase III; we shall also maintain the ordering of the parameters t_i in each phase respecting

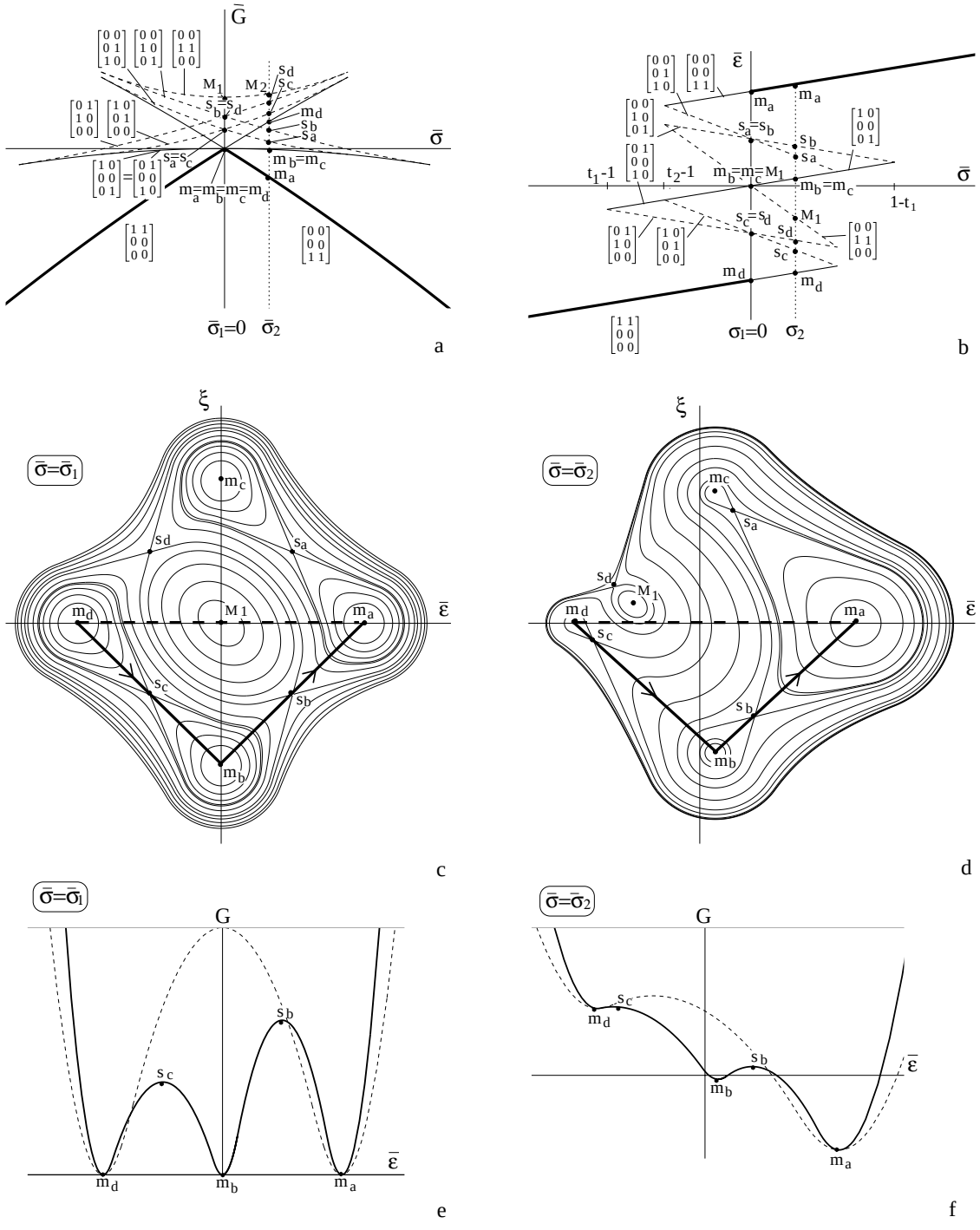

Fig. 5a–f. Potential energy landscapes for an inhomogeneous chain with $n = 2$. In **c** and **d** the "minimal barrier" paths (3.1, 3.2) are represented by the bold lines. The behavior of the potential energy along these paths (Peierls landscape) and along the path $\xi = 0$ (Cauchy-Born landscape, dashed lines) is compared in **e** and **f**. Here $t_1 = 0.75$, $t_2 = 0.85$, and $\sigma_M = 0$

$t_i < t_{i+1}$, $i = 1, \dots, \hat{k} - 1$, and $t_i < t_{i+1}$, $i = \hat{k} + 1, \dots, n - 1$. As a result, the $\hat{k}$-th spring is the "weakest" in phase I and the strain configuration A takes the form

$$\varepsilon_i = \begin{cases} \tilde{\sigma} - 1, & i = 1, \dots, \hat{k}, \\ \tilde{\sigma} + 1, & i = \hat{k} + 1, \dots, n. \end{cases} \tag{3.3}$$

Following the intuition developed in low dimensional cases we consider a path leading away from the metastable state A with all springs fixed except for the "weakest" in phase I, which changes phase. Choosing the overall strain $\bar{\varepsilon}$ as a parameter, we obtain

$$\varepsilon_i(\bar{\varepsilon}) = \begin{cases} \tilde{\sigma} - 1, & i = 1, \dots, \hat{k} - 1, \\ \hat{\varepsilon}_{\hat{k}}(\bar{\varepsilon}), & \\ \tilde{\sigma} + 1, & i = \hat{k} + 1, \dots, n. \end{cases} \tag{3.4}$$

In the phase space the trajectory (3.4) connects the local minimum A to the saddle S (with the $\hat{k}$-th spring shifted into the spinodal state II) and further to the local minimum B (with the $\hat{k}$-th spring already in phase III). Along this path all springs other than the $\hat{k}$-th remain in equilibrium with the applied force. In Appendix I we show that, exactly as in the simplest example $n = 2$, the saddle S corresponds to the smallest energy barrier in the neighborhood (basin) of the metastable state A. One can also verify that the trajectory (3.4) follows the line of steepest descent from the saddle S to the local minimum B. Indeed for $i \neq \hat{k}$ both $\varepsilon_i'(\bar{\varepsilon}) = 0$ and $\dfrac{dG}{d\varepsilon_i}(\varepsilon_i(\bar{\varepsilon})) = a(\dfrac{d\varphi_i}{d\varepsilon_i}(\varepsilon_i(\bar{\varepsilon})) - \bar{\sigma}) = 0$, and therefore the two vectors $\{\varepsilon_i'(\bar{\varepsilon})\}$ and $\nabla G(\varepsilon_i(\bar{\varepsilon}))$ are parallel.

To find the height of the minimal barrier we first check that the energy increases from A to S and decreases from S to B. Indeed, consider the potential energy of the i-th spring $g_i(\varepsilon_i) := a(\varphi_i(\varepsilon_i) - \bar{\sigma}\varepsilon_i)$ and write

$$g_i(\varepsilon^I) = g^I := -a\left(\frac{\tilde{\sigma}^2}{2} - \tilde{\sigma}\right), \quad g_i(\varepsilon^{II}) = \frac{a}{2}\left(-\frac{t_i}{t_i - 1}\tilde{\sigma}^2 + 1 - t_i\right), \quad g_i(\varepsilon^{III}) = g^{III} := -a\left(\frac{\tilde{\sigma}^2}{2} + \tilde{\sigma}\right).$$

The potential energy of the whole chain along the path (3.4) can now be written as a function of the overall strain

$$G(\bar{\varepsilon}) = (\hat{k} - 1)g^I + g_{\hat{k}}(\varepsilon_{\hat{k}}(\bar{\varepsilon})) + \hat{m}g^{III}. \tag{3.5}$$

The desired conclusion follows if, using $(2.3)_1$, we compute the derivative $G'(\bar{\varepsilon}) = L(\varphi_{\hat{k}}'(\bar{\varepsilon}) - \bar{\sigma})$. The energy barrier is equal to

$$h_{\hat{k}}(\tilde{\sigma}) = \frac{L}{2n}\frac{(\tilde{\sigma} + t_{\hat{k}} - 1)^2}{1 - t_{\hat{k}}}. \tag{3.6}$$

Now, by arranging a sequence of n segments (3.4), we obtain a complete transition from the homogeneous state $k = n$ (phase I) to the homogeneous state $k = 0$ (phase III). Along this "synthetic" path the springs change phase one at a time starting from the "weakest", $\hat{k} = n$, to the "strongest", $\hat{k} = 1$. The energy barriers (3.6), associated with successive transitions, increase as the transformation advances from the spring $\hat{k} = n$ with the largest value of $t_{\hat{k}}$ to the spring $\hat{k} = 1$ with the smallest value of $t_{\hat{k}}$. Since the springs are ordered according to their "strength", the successive switching events may be viewed as a propagation of the transformation front. We illustrate the relevant "Peierls landscape" of a typical inhomogeneous chain with $n = 5$ in Fig.6.

4 Transformation mechanism

In this section we apply the knowledge of the energy landscape to explore possible scenaria of phase transition in the "driven" inhomogeneous chain when applied load increases or decreases quasi-statically. We assume that due to the presence of external fluctuations the system escapes from a metastable state as soon as the minimal energy barrier in its neighborhood falls below a given threshold $h = \hat{h}$; after reaching an appropriate saddle, the system relaxes to a new metastable state following the steepest descent path.

To be specific, consider a metastable configuration A (from Sect. 3) with $\hat{k}$ springs in phase I and with strains of individual springs as in (3.3). The "minimal barrier path" is then given by (3.4). The transition

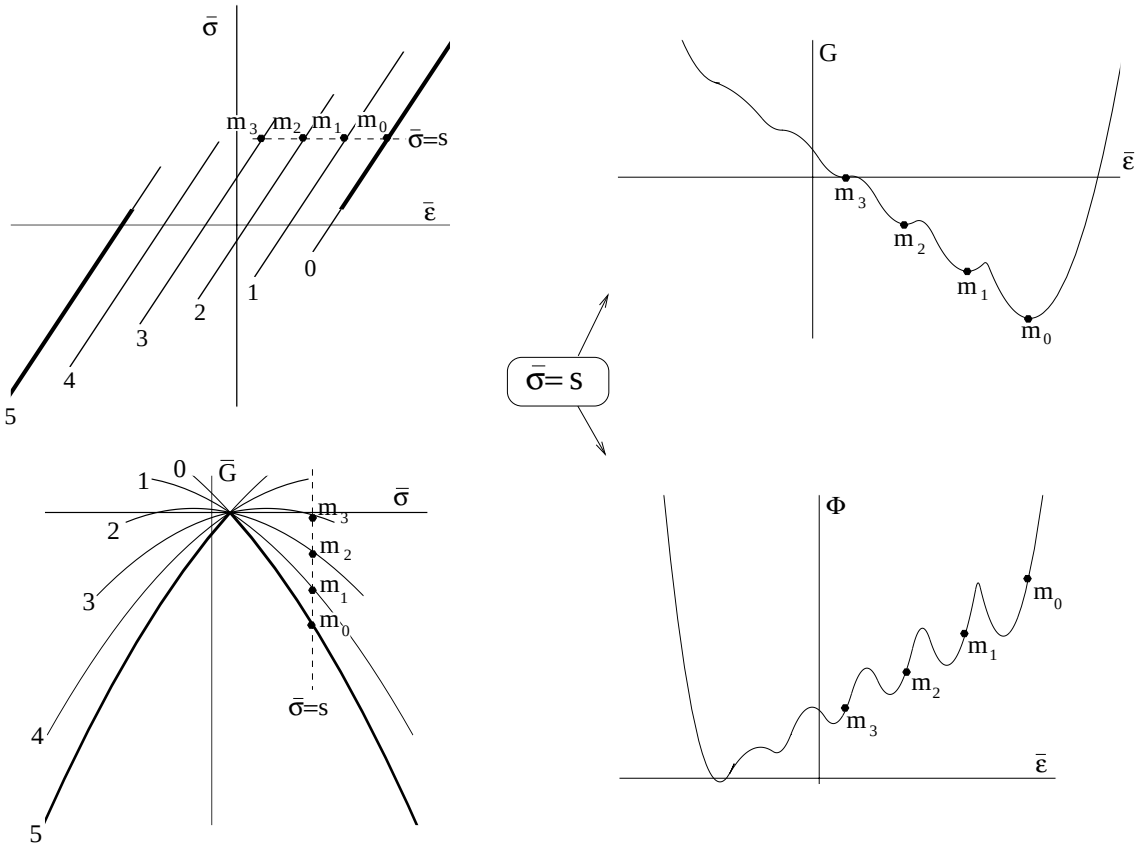

Fig. 6. Peierls energy landscapes for a chain with $n = 5$ loaded by a fixed force s. Here $\sigma_M = 0.1$, $s = 0.45$, $\beta = 5$, and $t_0 = 1/2$

process can be viewed as consisting of two steps. First, the metastable system absorbs the activation energy $\hat{h}$ and reaches the optimal "excited" state S, with one spring shifted into the spinodal region. Then the resulting unstable configuration instantly breaks up giving rise to a new metastable state B with lower energy. The released energy may be decomposed into the activation part $G(S) - G(A) = \hat{h}$ which is returned to the system and the excess part

$$Q_{\hat{k}} = G(A) - G(B) = 2a\tilde{\sigma}_{\hat{k}} \tag{4.7}$$

which is assumed to dissipate irreversibly. Here

$$\tilde{\sigma}_{\hat{k}} = 1 - t_{\hat{k}} - \sqrt{2n\hat{h}(1 - t_{\hat{k}})/L} \tag{4.8}$$

is the corresponding value of the force, specified by $\hat{h}$ (see (3.6)).

Notice that in the transformation process the elastic energy Φ also changes so that a part of the external work remains stored in the system. For the stored elastic energy, which can be loosely identified with the energy of "cold work", we obtain

$$[\![\bar{\Phi}]\!]_{\hat{k}} = 2a\sigma_M . \tag{4.9}$$

Since in our model the value of the Maxwell force σ_M is assumed to be the same for all springs, the total cold work acquired in the transformation process depends only on the number of transformed springs.

The overall mechanical behavior of the chain depends on the choice of the activation energy $\hat{h}$. Two cases of special interest are the case of global minimization and the case of maximal delay. In the first case the system is assumed to overcome the largest of the barriers at Maxwell force: $h_k^{max} = \frac{L}{2n}(1 - t_k)$. Due to our specific ordering of the springs properties, this scenario takes place when $\hat{h} \geq h_1^{max}$. In the second case the threshold is the smallest, $\hat{h} = 0$, and the system is unable to overcome any barriers at all.

Consider now a generic case

$$0 < \hat{h} < h_n^{max} \tag{4.10}$$

when the transition force for each spring is higher than the Maxwell force. Suppose that the load is increasing starting from some value $\tilde{\sigma} < 0$ when the only minimum of the energy is the configuration with all springs in phase I ($k = n$). As long as $\tilde{\sigma} < 0$ all the inhomogeneous metastable states have higher energy than the homogeneous state. At the Maxwell force, $\tilde{\sigma} = 0$, alternative low energy metastable states become available, however the barriers between them and the initial state are still too high for the transformation to take off. The chain then behaves elastically until the lowest transition force $\tilde{\sigma}_n$ is reached and the system can exit the basin of the homogeneous state $k = n$. The transformation then proceeds along the "minimal barrier path" with the "weakest" spring ($i = n$) changing phase while the other springs remain fixed. Eventually the system reaches a new metastable state with $k = n - 1$ springs in phase I. The force required to exit this new metastable state depends now on the parameter t_{n-1}; the system again behaves elastically until at $\tilde{\sigma} = \tilde{\sigma}_{n-1}$ the next "weakest" spring is ready to change phase.

As the load increases further, other springs change phase one at a time in the order of their relative "strength". Meanwhile the system experiences an alternate sequence of elastic deformations and abrupt strain discontinuities, until all springs end up in phase III. In Fig. 7 we illustrate the overall response of the system in the force-strain space. We remark that the distinctive "staircase" structure of the force-strain curve is reminiscent of the Portevin-Le Chatelier effect (e.g. [4], [37]).

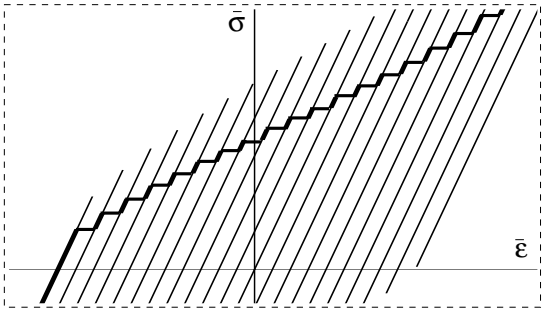

Fig. 7. Portevin-Le Chatelier effect. Bold line represents the "minimal barrier path" followed by the chain with the same parameters as in Fig. 4 in the presence of external activation $0 < \hat{h} < h_{\max}$

If the load is reversed the evolution pattern is essentially the same modulo elastic unloading. Thus, starting from a homogeneous configuration III the system behaves elastically until at $\tilde{\sigma} = -\tilde{\sigma}_n$ the "weakest" spring $i = n$ switches back to phase I (notice the Bauschinger effect!). The next barrier is again higher and the system behaves elastically until the next "weakest" spring changes phase. Due to the symmetry of the energy, the reverse transitions are accompanied by the same dissipation, $Q_k^- = 2a\tilde{\sigma}_k$, while the cold work of the reverse transitions has the opposite sign $[\![\bar{\Phi}]\!]_k = -2a\sigma_M$. One can see that during the reverse transition the system completely returns the cold work (4.9) acquired in the direct transition, while the overall dissipation remains strictly positive.

We conclude this section with a few remarks concerning the possibility to formulate the phase transition criterion in terms of the relevant driving (or configurational) force. To introduce the concept of the driving force in the present context, we recall that when the $\hat{k}$-th spring changes phase from phase I to III its strain jumps according to $[\![\varepsilon_{\hat{k}}]\!] = \varepsilon^{III}(\tilde{\sigma}_{\hat{k}}) - \varepsilon^{I}(\tilde{\sigma}_{\hat{k}}) = 2$. The driving force f for this transition can then be defined as $f := \dfrac{Q_k}{a[\![\varepsilon_{\hat{k}}]\!]} = \tilde{\sigma}$. Notice that it does not depend on the index of the spring that changes phase. If we now consider a simultaneous transition of l springs, the dissipated energy is $Q(l) = 2al\tilde{\sigma}$ and the total elongation is $\sum a[\![\varepsilon]\!] = 2al$, so that the driving force does not depend on the number of transformed springs. We conclude that in our model a criterion based on a given threshold for the driving force would not distinguish between "weak" and "strong" springs, between one and many, forcing all switching events to take place at the same value of the external force. The chain would then behave as in the homogeneous case studied in [27] with no hardening or Bauschinger effect whatsoever. To recover those effects in the framework of the driving force criterion one would need to reinstate the inhomogeneity of the Maxwell force σ_M.

5 Hysteresis

In this section we study the fine structure of the hysteresis for a chain subjected to a cyclic loading. As we have shown in the previous sections, given the activation energy $\hat{h}$ one can identify for each spring k the force at which it changes phase: $\tilde{\sigma}_k$ for increasing load and $-\tilde{\sigma}_k$ for decreasing load. It is then clear that what determines the phase configuration of the chain is the succession of maxima and minima on the loading history curve. We denote these load reversal points as s^i and s_i, accordingly; here i represents the number of the cycle.

5.1 Examples

The hysteretic behavior of the simplest chain with two springs is illustrated in Fig. 8 for the case $0 < \hat{h} < h_1^{max}$. Suppose that we start with the equilibrium homogeneous configuration with both springs in phase I and $k = 2$. As the load increases the system follows the path *a-b-c-d-e* which eventually brings it to the other homogeneous configuration with both springs in phase *III* and $k = 0$. If then the load is lowered, the system undergoes a reverse transition and follows the path *e-g-h-i-a*. The internal loops are recovered if the load is reverted before the transformation is complete. For example, the cycle *n-b-c-m-n* is obtained for unloading beginning at $s^1 \in (\tilde{\sigma}_2, \tilde{\sigma}_1)$.

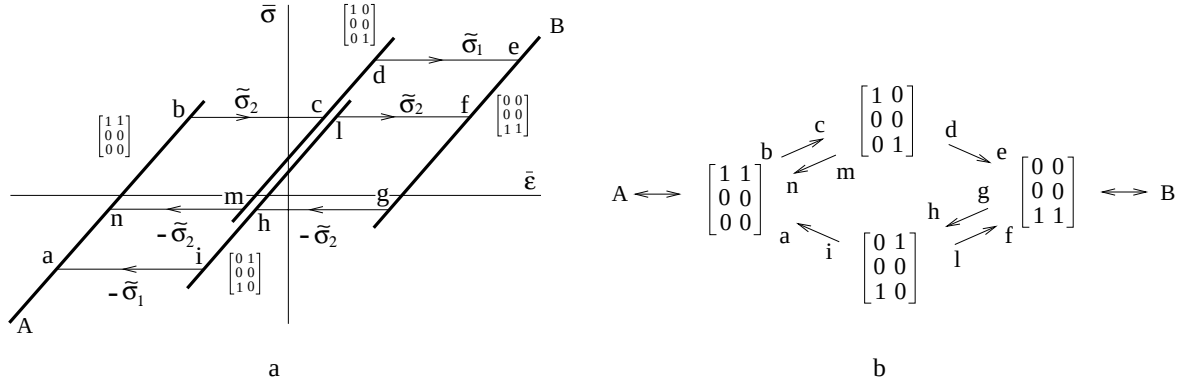

a b

Fig. 8a,b. Inner and outer hysteresis loops for the simplest chain with $n = 2$ **a**. For clarity the two (superimposed) two-phase branches ($k = 1, l = 0, m = 1$) have been separated. In **b** the same loops are represented in the phase space χ_i^α. Here $\sigma_M = 0.2$, $t_1 = 0.2$, and $t_2 = 0.6$

In the case $n = 3$ the loop anatomy is illustrated in Fig. 9. One can see that there exist three (congruent) internal cycles of small size (*a-b-s-r*, *b-t-l-s*, *t-h-i-l*), two (congruent) internal cycles of medium size (*q-a-b-c-d-l-s-n-q*, *n-c-d-e-f-i-l-m-n*), and one large external cycle. To follow just one segment, we observe that the point s in the force-strain space in Fig. 9a corresponds to three different phase configurations denoted by s_1, s_2, s_3 . Hence, if the unloading starts at s the phase switches inside individual elements take place at either *s*, *n*, or *o*, depending on the initial phase configuration (non-local memory in the terminology of [5]). Notice also that under two different initial conditions l_1 and l_2 the chain may first follow one path (*l-s-n*) and only later bifurcate into two different paths (*n-q* and *n-o-p*).

5.2 General case

As we have already noticed, the memory of our system is restricted to the load reversal points s^i and s_i. In particular the system changes phase only if $s^i \geq \tilde{\sigma}_n$, or $s_i \leq -\tilde{\sigma}_n$. Reaching the load s^i means that all springs with $\tilde{\sigma}_k \leq s^i$ have already transformed into phase *III* and similarly reaching the load s_i means that all springs with $-\tilde{\sigma}_k \geq s_i$ are in phase I. Consequently, the overall strain is completely defined by the decreasing subsequences of past local maxima $s^i > \tilde{\sigma}_n$ and increasing subsequences of past local minima $s_i < -\tilde{\sigma}_n$. Moreover, each local maximum $s^i \geq \tilde{\sigma}_n$ deletes the memory of all preceding load reversals $s^j \in (\tilde{\sigma}_n, s^i)$ and

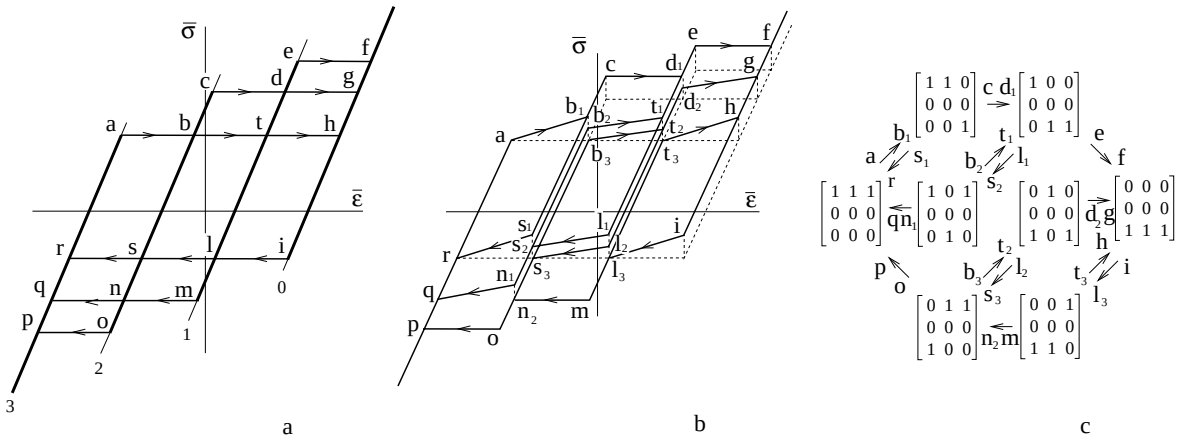

Fig. 9a–c. Inner and outer hysteresis loops for a chain with $n = 3$ (**a**, **b**). In **c** the same trajectories are shown in the phase space χ_i^α. Here $\sigma_M = 0.05$, $t_1 = 0.4$, $t_2 = 0.6$, and $t_3 = 0.8$

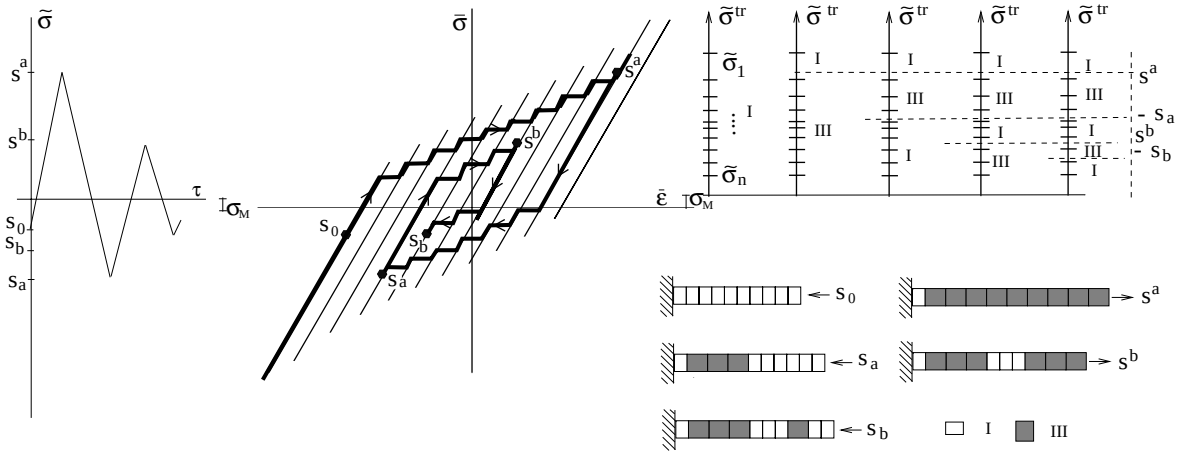

Fig. 10. A loading history with decreasing reversal loads illustrating the process of creation of new "interfaces". Here $n = 10$, $\sigma_M = 0.1$, $\beta = 5$, $t_0 = 0.5$

$s_j \in (-s^i, -\tilde{\sigma}_n)$ for all $j < i$ ("wiping out" property). In Fig. 10 we illustrate a typical evolution path for a chain with $n = 10$ loaded by an oscillatory force with decreasing amplitude; since $s^a > |s_a| > s^b > |s_b|$, the memory of all load reversals is preserved.

One can see that the reversal points with $s^i \geq \tilde{\sigma}_n$ and $s_i \leq -\tilde{\sigma}_n$ create new "interfaces". When one interface meets another, they annihilate and the memory of the corresponding reversal load gets lost. By using the "wiping out" property one can conclude that for "closed-loop" loading histories the parameters of the system also follow closed loop trajectories (*return point memory*). This important property is proved in the Appendix *II*. It is illustrated in Fig. 11 where the loading $s_0 \to s^a \to s_a \to s^b = s^a$ produces a closed loop in the force-strain space: at $\tilde{\sigma} = s^b$ the system returns into the same configuration from where it started at $\tilde{\sigma} = s^a$. In addition Fig. 11 shows two congruent cycles obtained from two different initial conditions. One can see that these identical loading histories generate congruent loops independently of the initial configuration (*congruency property*). The fact that this property is necessary is also proved in the Appendix *II*.

6 Continuum limit

In this section we study the behavior of the chain in the limit when the number of springs goes to infinity, $n \to \infty$. We assume that the total length of the resulting continuous "bar" is finite, $na = L$, which means that

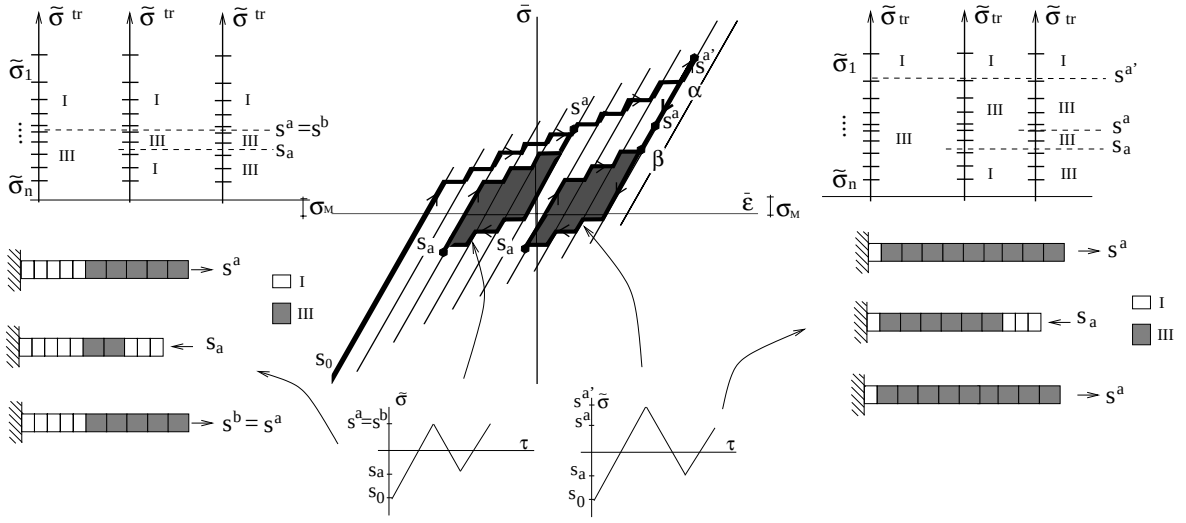

Fig. 11. Return point memory and congruency properties. Due to our simplifying assumption that the Maxwell force σ_M is the same for all springs, all inner loops are "centered" around the axis $\tilde{\sigma} = \sigma_M$ and each inner loop is connected to the outer loop by an elastic branch (segment $\alpha - \beta$). The parameters are the same as in Fig. 10

$a \to 0$ and the springs become infinitely small. To characterize the inhomogeneity in the limiting problem we use a continuous distribution $t = \hat{t}(x)$, $x \in (0, L)$, with imposed monotonicity condition $\hat{t}\,'(x) > 0$.

6.1 The model

In the limiting problem the role of the index i is played by the continuous coordinate $x \in (0, L)$. The configuration of the chain is characterized by the phase functions $\chi^\alpha(x)$ equal to 1 when section x is in phase α and 0 otherwise. Since in the metastable configurations the springs are allowed to be in phases I and III only, it is sufficient to use a single characteristic function $\chi^I(x)$. One can also define a continuum analog of the phase fraction $\mu = \dfrac{1}{L}\displaystyle\int_{\mathscr{I}_x^I} dx$, where $\mathscr{I}_x^\alpha = \{x \in (0, L) : \chi^\alpha(x) = 1\}$.

By adopting the new variables, we can rewrite the expressions for the parameters of the metastable equilibria in the form

$$\bar{\varepsilon} = \tilde{\sigma} + \varepsilon_0\,, \quad \bar{\Phi} = \frac{L}{2}\tilde{\sigma}^2 + L\sigma_M\,\bar{\varepsilon}(\tilde{\sigma}), \quad \bar{G} = -L\frac{\tilde{\sigma}}{2} - L\tilde{\sigma}\varepsilon_0\,, \tag{6.1}$$

where now $\varepsilon_0 = 1 - 2\mu$. As in the discrete case (2.4), the inhomogeneity distribution does not enter these relations explicitly and determine only the limits of stability for the equilibrium branches.

We remark that in the continuum limit the energy landscape remains "wiggly" even though the heights of the energy barriers between the neighboring local minima tend to zero. To obtain a meaningful limit for the deformation paths considered in the previous sections, we need to assume that the activation energy per spring also goes to zero, $\hat{h} \to 0$, while the total activation energy available to the system remains finite $\hat{h}n = \hat{H}$. Here $\hat{H}$ is a given constant, playing the same role as $\hat{h}$ in the discrete problem. Following (4.10) we assume that $\hat{H} < (1 - \bar{t})L/2$, where $\hat{t}(x) < \bar{t} < 1$, which guarantees that the transformation does not start before the Maxwell force is attained.

The expression for the force required to transform a section $x \in (0, L)$ follows from (4.8)

$$\tilde{\sigma}^{tr}(x) = 1 - \hat{t}(x) - \sqrt{2\hat{H}(1 - \hat{t}(x))/L}\,. \tag{6.2}$$

It can be inverted to give

$$\hat{t}(\tilde{\sigma}^{tr}(x)) = 1 - \tilde{\sigma}^{tr}(x) - \frac{\hat{H}}{L} - \frac{\sqrt{\hat{H}^2 + 2L\hat{H}\,\tilde{\sigma}^{tr}(x)}}{L}. \tag{6.3}$$

Since the correspondence between $t = \hat{t}(x)$ and the transformation stresses $\tilde{\sigma} = \tilde{\sigma}(x)$ is one to one, in addition to $\mathscr{T}_x^I$ one can introduce equivalent sets in $\tilde{\sigma}$ and t spaces, $\mathscr{T}_\sigma^I$ and $\mathscr{T}_t^I$ correspondingly. Now to compute ε_0 one can use any of the following formulas

$$\varepsilon_0 = 1 - \frac{2}{L}\int_{\mathscr{T}_x^I} dx = 1 - 2\int_{\mathscr{T}_t^I} p(t)dt = 1 - 2\int_{\mathscr{T}_\sigma^I}\left(\frac{\sqrt{\hat{H}}}{\sqrt{\hat{H} + 2\tilde{\sigma}^{tr}L}} + 1\right) p(\hat{t}(\tilde{\sigma}^{tr}))d\tilde{\sigma}^{tr}. \tag{6.4}$$

Consider a loading path $\tilde{\sigma} = \tilde{\sigma}(\tau)$ which begins with a homogeneous configuration $\chi^I(x) \equiv 1$. We indicate again by s^i successive maxima and by s_i successive minima of the external force, $i = a, b, c, \ldots$. The subsequent configurations of the system may be determined only in an incremental way, reminiscent to the procedures adopted in the classical plasticity theory. Thus, we know that by the time $\tilde{\sigma}(\tau) = s^a$ the set $\{x \in (0, L) : \tilde{\sigma}^{tr}(x) \le s^a\}$ has already transformed into phase *III* and $\mathscr{T}_\sigma^I = \mathscr{T}_\sigma^I(s^a) := \{\tilde{\sigma}^{tr} \in (0, 1) : \tilde{\sigma}^{tr} > s^a\}$. As a result an "interface" (*i.e.* a discontinuity of the phase function χ^I) has formed between phases *I* and *III* and moved at a location x^a satisfying $\tilde{\sigma}^{tr}(x^a) = s^a$. Notice that due to our assumption $\hat{t}\,'(x) > 0$ the first interface nucleates at $x = L$ and then propagates inside the "bar". Suppose now that the load is reverted. In the process of purely elastic unloading the "bar" deforms according to $\bar{\varepsilon}(\tilde{\sigma}(\tau)) = \tilde{\sigma}(\tau) + \varepsilon_0(s^a)$ and the reverse phase transition does not start until $-\tilde{\sigma}(\tau) = -\tilde{\sigma}^{tr}(\bar{t}) < 0$. The parameter $\varepsilon_0(s^a)$ can be found from (6.4) with $\mathscr{T}_\sigma^I = \mathscr{T}_\sigma^I(s^a)$. As the reverse transformation begins, another interface nucleates at $x = L$ and propagates inside the "bar". If $|s_a| < s^a$, by the time $\tilde{\sigma}(\tau) = s_a$ the set $\{x \in (0, L) : \tilde{\sigma}^{tr}(x) \le |s_a|\}$ transforms back into phase *I* with the formation of an interface at x_a satisfying $\tilde{\sigma}^{tr}(x_a) = s_a$. If instead $|s_a| > s^a$ the whole "bar" transforms back to phase *I* at $\tilde{\sigma}(\tau) = -s^a$. Notice that in this case the memory of the reversal point s^a has been erased.

To summarize, reaching a reversal point with $s^i \ge \tilde{\sigma}^{tr}(\bar{t})$ ensures the transformation of the set $\{x \in (0, L) : \tilde{\sigma}^{tr}(x) \le s^i\}$ into phase *III* while achieving a reversal point with $s_i \le -\tilde{\sigma}^{tr}(\bar{t})$ guarantees that the set $\{x \in (0, L) : \tilde{\sigma}^{tr}(x) \le |s_i|\}$ is in phase *I*. By the same reasoning as in the discrete case, one can show that the behavior of the continuous system is consistent with the return point memory, wiping out, and the congruency properties (see Fig. 12c). The resulting picture is presented in Fig. 12a where we illustrate the behavior of the continuous system under quasi-static cyclic loading. To insure that the memory of no reversion point is deleted we assumed that the oscillatory applied force has a decreasing amplitude. One can see, that the deformation field is piecewise homogeneous: the "bar" is divided into segments occupied by phases *I* and *III* and separated by interfaces where the strain $\bar{\varepsilon} = \bar{\varepsilon}(x)$ changes abruptly. Since the springs are now infinitely small one can not distinguish elastic and plastic steps, which is characteristic for a material with continuous hardening.

6.2 Cold work and dissipation

Consider now the decomposition of the external work into the energy of "cold work" and the dissipated component. We recall that in our discrete problem the dissipation is taking place exclusively during the switching events inside the individual elements in analogy with the dissipative slip events in conventional plasticity. The accompanying acquisition or release of cold work is associated with the fact that in those transitions the elastic energy can go up or down. Here the analogy with plasticity theory is somewhat less obvious since "plastic" wells in the actual crystal must be identical. We may comment, however, that the passage of a dislocation through a finite crystal creates (or eliminates) a finite step on the boundary which may be interpreted as switching to a well with a slightly different energy. In spite of this our one dimensional model is still too crude to capture the main component of the cold work associated with the energy of the defects trapped inside the crystal.

As we have already mentioned, in the continuum limit the distinction between elastic and plastic steps is erased and we have to deal with derivatives instead of finite jumps. When the loading path $\tilde{\sigma} = \tilde{\sigma}(\tau)$ is given, we can use $\tilde{\sigma}$ as a parameter and compute

$$\frac{dW}{d\tilde{\sigma}} = L\bar{\sigma}\frac{d\bar{\varepsilon}}{d\tilde{\sigma}} = L\frac{\bar{\sigma}}{E(\tilde{\sigma})}, \qquad \frac{d\bar{\Phi}}{d\tilde{\sigma}} = L\left(\tilde{\sigma} + \frac{\sigma_M}{E(\tilde{\sigma})}\right), \qquad \frac{dQ}{d\tilde{\sigma}} = \frac{dW}{d\tilde{\sigma}} - \frac{d\bar{\Phi}}{d\tilde{\sigma}} = L\tilde{\sigma}\left(\frac{1}{E(\tilde{\sigma})} - 1\right). \tag{6.5}$$

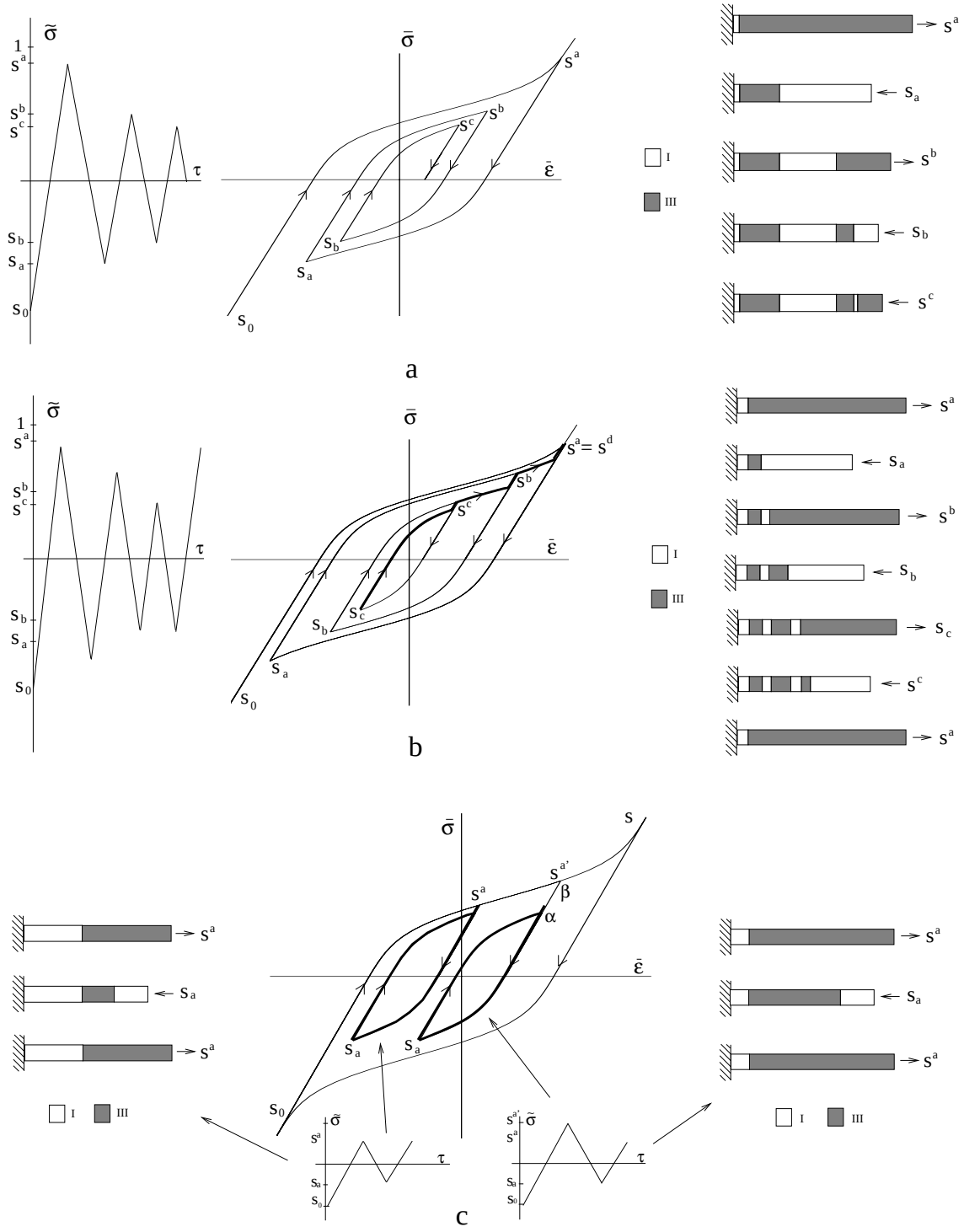

Fig. 12a–c. Hysteresis in the limiting continuous system. Here $\hat{H} = 0$ (maximum delay convention), $\sigma_M = 0$, $\beta = 20$, and $t_0 = 0.5$

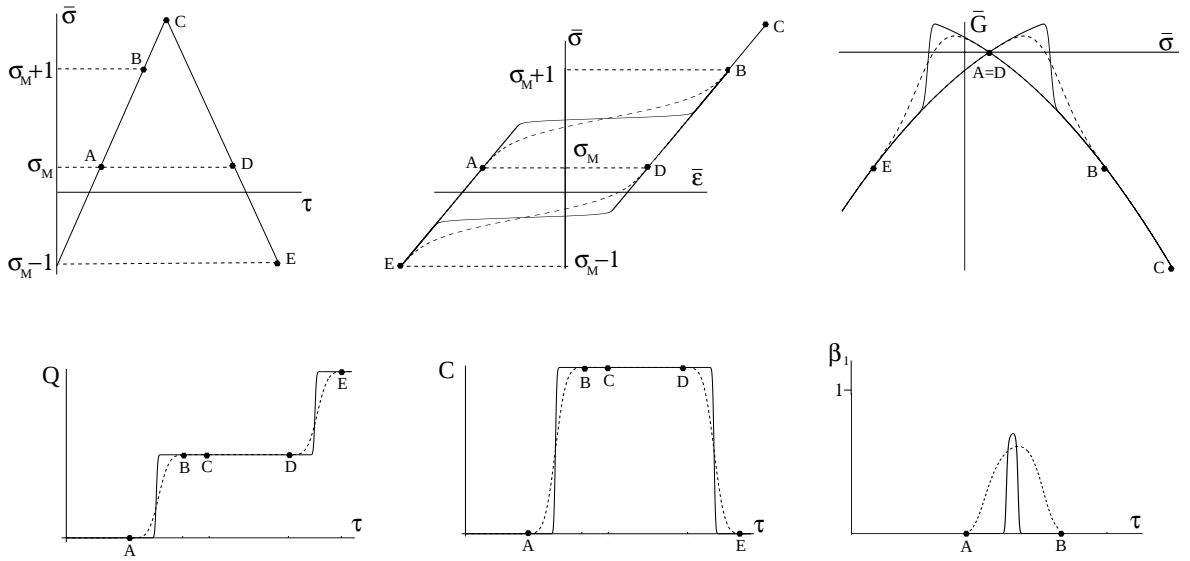

Fig. 13. Behavior of the potential energy $\bar{G}$, dissipated energy Q, cold work C, and coefficient β_1 in a complete hysteresis cycle for two chains with different degree of inhomogeneity: $\beta = 20$ (*dashed lines*) and $\beta = 1000$ (*solid lines*). Here $t_0 = 0.5$ and $\sigma_M = 0.2$

Here W is the work of the loading device, $\bar{\Phi}$ is the elastic energy, and Q is the dissipated energy. Since $\varphi(\varepsilon^I) - \varphi(\varepsilon^{III}) = -2\sigma_M$, for the cold work C we obtain

$$\frac{dC}{d\tilde{\sigma}} = -2L\sigma_M \frac{d\mu}{d\tilde{\sigma}} = L\sigma_M \frac{d\varepsilon_0}{d\tilde{\sigma}} = L\sigma_M \left(\frac{1}{E(\tilde{\sigma})} - 1\right).$$

In the above formulas the tangent modulus $E(\tilde{\sigma})$ contains both elastic and "plastic" contributions. It can be computed from the definition $E^{-1}(\tilde{\sigma}) := \dfrac{d\bar{\varepsilon}}{d\tilde{\sigma}}(\tilde{\sigma}) = 1 + \dfrac{d\varepsilon_0}{d\tilde{\sigma}}(\tilde{\sigma})$ if the corresponding derivatives are known. Given that during the "elastic" stages the phase fractions remain fixed we obtain that $\dfrac{d\varepsilon_0}{d\tilde{\sigma}}(\tilde{\sigma}) = 0$ and $E(\tilde{\sigma}) = 1$. For the "plastic" stages we obtain

$$\frac{d\varepsilon_0}{d\tilde{\sigma}}(\tilde{\sigma}) = \frac{d\varepsilon_0}{d\tilde{\sigma}^{tr}} \frac{d\tilde{\sigma}^{tr}}{d\tilde{\sigma}}(\tilde{\sigma}) = -2\left(\frac{\sqrt{\hat{H}}}{\sqrt{\hat{H} + 2\tilde{\sigma}_{tr}L}} + 1\right) p(\hat{t}(|\tilde{\sigma}|)) \frac{d\,\mathrm{meas} I^I_\sigma}{d\tilde{\sigma}^{tr}} \frac{d\tilde{\sigma}^{tr}}{d\tilde{\sigma}}.$$

Now, if the stress is increasing and $\tilde{\sigma}_{tr} = \tilde{\sigma} > 0$, the measure of the set I^{III}_σ is also increasing while the measure of its complement I^I_σ is decreasing. More specifically $\dfrac{d\,\mathrm{meas} I^{III}_\sigma}{d\tilde{\sigma}^{tr}} = -\dfrac{d\,\mathrm{meas} I^I_{\sigma^{tr}}}{d\tilde{\sigma}^{tr}} = 1$. If, on the contrary, the stress is decreasing, and $\tilde{\sigma}_{tr} = -\tilde{\sigma} > 0$, we obtain $\dfrac{d\,\mathrm{meas} I^I_\sigma}{d\tilde{\sigma}} = 1$. In the general case

$$E(\tilde{\sigma}) = \begin{cases} 1, & \text{elastic range,} \\ \left(1 + 2\left(\dfrac{\sqrt{\hat{H}}}{\sqrt{\hat{H} + 2|\tilde{\sigma}|L}} + 1\right) p(\hat{t}(|\tilde{\sigma}|))\right)^{-1}, & \text{plastic range.} \end{cases} \tag{6.6}$$

With these formulas we can explicitly compute the fractions of external work dissipated, stored, and transformed into the energy of cold work

$$\beta_1 := \frac{dQ/d\tilde{\sigma}}{dW/d\tilde{\sigma}} = \frac{\tilde{\sigma}}{\bar{\sigma}}(1 - E(\tilde{\sigma})), \beta_2 := \frac{d\Phi/d\tilde{\sigma}}{dW/d\tilde{\sigma}} = \frac{\tilde{\sigma}E(\tilde{\sigma}) + \sigma_M}{\bar{\sigma}}, \beta_3 := \frac{dC/d\tilde{\sigma}}{dW/d\tilde{\sigma}} = \frac{\sigma_M(1 - E(\tilde{\sigma}))}{\bar{\sigma}}.$$

Some of the results are illustrated in Fig. 13 for a typical cycle of loading and unloading. Notice that the ratio β_1 is not constant during the plastic stages. Instead its variation is controlled by the inhomogeneity

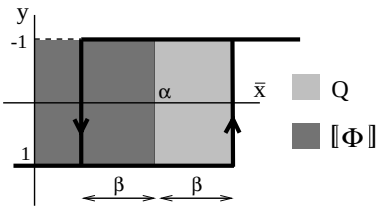

Fig. 14. Hysteresis operator in the Preisach model

distribution $p = p(t)$ through (6.6). We recall that in classical thermo-plasticity the parameter analogous to β_1 is assumed to be constant, which agrees with the prediction of our model in the homogeneous case [27]. Recent experiments on metal plasticity, reported in [29], reveal that β_1 may vary with strain; according to our model this variation of β_1 may be used as a measure of internal inhomogeneity.

6.3 Equivalent Preisach model

In the previous section we have shown that both our discrete system and its continuous analog exhibit return point memory and congruency properties. These features are known to be sufficient for a hysteretic system to have a description in terms of the Preisach model [14]. The Preisach model was originally introduced as a formal interpolation scheme for the ferromagnetic hysteresis [5]. More recently it has been used for the description of rate independent hysteresis in a variety of solid materials including shape memory alloys (e.g. [22]).

In Preisach modeling one starts with the introduction of a continuous distribution of non-interacting bi-stable elements subjected to the action of an external field. Each bi-stable element can be in two states $y = \pm 1$; the particular configuration of an element depends on an input parameter $\bar{x}$ (external field) through a hysteretic operator schematically shown in Fig. 14. The overall response of the system is nontrivial only when different Preisach elements have different constitutive parameters α and β. Suppose that the distribution of the element properties is characterized by a probability density $q = \bar{q}(\alpha, \beta)$ which satisfies $\int_{\mathscr{R}} \bar{q}(\alpha, \beta)\, d\alpha\, d\beta = 1$. If we denote by $\mathscr{R}_+$ the region in the (α, β) space where $y = 1$ and by $\mathscr{R}_-$ its complement in $\mathscr{R}$, the overall input-output constitutive relation for the Preisach model takes the form

$$\bar{y}(\bar{x}) = \int_{\mathscr{R}_+} \bar{q}(\alpha, \beta)\, d\alpha\, d\beta - \int_{\mathscr{R}_-} \bar{q}(\alpha, \beta)\, d\alpha\, d\beta = 1 - 2 \int_{\mathscr{R}_-} \bar{q}(\alpha, \beta)\, d\alpha\, d\beta. \tag{6.7}$$

To explicate the analogy between Preisach model and our discrete mechanical chain it is sufficient to replace the input parameter $\bar{x}$ of the Preisach model by our applied force $\bar{\sigma}$, the elemental variables y by our strains ε_i, and the output parameter $\bar{y}$ by our overall strain $\bar{\varepsilon}$. The parameters α and β can then be identified as the Maxwell force σ_M and the transformation stress $\tilde{\sigma}_k$. The equivalent Preisach distribution will then take the form $\bar{q}(\alpha, \beta) = \delta(\alpha - \sigma_M)\bar{q}(\beta)$ with

$$\bar{q}(\beta) = \left(\frac{\sqrt{\hat{H}}}{\sqrt{\hat{H} + 2\beta L}} + 1 \right) p(\hat{t}(\beta)).$$

To reproduce our continuous hysteresis loops described by $(6.1)_1$ and (6.4), we need to add to (6.7) a new, purely elastic term

$$\begin{aligned} \bar{\varepsilon}(\tilde{\sigma}(\tau)) &= \tilde{\sigma} + 1 - 2 \int_{\mathscr{R}^-} \delta(\alpha - \sigma_M)\bar{q}(\beta)\, d\alpha\, d\beta \\ &= \tilde{\sigma}^{tr} + 1 - 2 \int_{\mathscr{T}^l_\sigma} \left(\frac{\sqrt{H}}{\sqrt{H + 2\tilde{\sigma} L}} + 1 \right) p(\hat{t}(\tilde{\sigma}^{tr}))\, d\tilde{\sigma}^{tr}. \end{aligned} \tag{6.8}$$

It is now easy to show that through this *aposteriori* construction, we obtain a "generalized" version of the Preisach model reproducing both outer and inner loops of our discrete model in the continuum limit. Despite this formal equivalence, realized above for specific "dynamics" which we called "minimal barrier strategy",

the discrete model is more general than any particular Preisach model adaptation. We recall that the bi-stable springs are not directly controlled by the applied force and that the energy relaxation is taking place in the presence of a multiplicity of metastable configurations. As a result, the mechanical model is compatible with a broad spectrum of alternative hysteretic patterns and, in particular, can generate strategies violating both the return point memory and the congruency properties.

7 Concluding remarks

Although discreteness and non-convexity of the elastic energy have been long realized as crucial for the description of rate independent hysteresis in "smart" materials, the typical models have been over-symmetrical in the sense that the elements were assumed to be identical. The main goal of the present paper was to eliminate this degeneracy and to explore the consequences of the simplest inhomogeneity in the system.

Specifically, we allowed the energy barriers separating the two phases to vary, distinguishing therefore elastic elements according to their "strength". Physically this may mean that some grains have preferential orientations and therefore transform at smaller stresses than others, or that a particular defect distribution makes certain transformation sites preferable. In real solids the effective "strength" of the elements may also increase with the progress of the transformation, as the accumulation of the transformation-related defects and dislocations make further advance of the deformation process more difficult. The main consequence of the inhomogeneity of the system appear to be hardening which can be viewed as a manifestation of the fact that the transformation advances from the "weakest" elements to the "strongest".

Discrete elastic systems with non-convex elements exhibit complex energy landscapes with multiple local minima. In order to predict the evolution of the transformation, the knowledge of the energy landscape is not sufficient and one needs to make assumptions of dynamical nature. In the present model we assumed, as a first approximation, that the dynamics is maximally dissipative. To increase the range of applications of the model we also assumed that there exists a fixed activation energy supplied from outside and that the system can escape from a metastable state whenever the minimal barrier around its basin falls below a fixed threshold. As we have shown, the resulting evolution, can be presented as a sequence of purely elastic, conservative steps interrupted by a succession of discontinuous, dissipative switching events. The corresponding "macroscopic" stress-strain curve exhibits a distinctive hardening pattern with serrations of "staircase" shape. If, in addition, the elements are ordered according to their strength, the transformation propagates as a localized front.

Despite the simplicity of the present approach, the resulting organization of the hysteresis loops is quite complicated and the model possesses a rich memory structure. In particular we have proved that the congruency and the return point memory properties are necessary consequences of our main assumptions. To compare our model with the more standard approaches to hysteresis, we constructed a generalized Preisach distribution reproducing both inner and outer hysteresis loops of our model. Despite the availability of this alternative representation, our model under various dynamic assumptions is capable of generating a much richer variety of evolution scenaria than any particular Preisach model.

We believe that the analogy of the transformational plasticity studied in this paper with the classical metal plasticity is more than superficial. It is enough to mention that the main section of the energy landscape relevant for the interpretation of our transformation mechanism is a direct analog of the Peierls landscape in the theory of dislocations. In spite of the many similarities reported in this paper there of course remain major differences, most importantly, due to the fact that in metal plasticity the basic nonlinear "elements" are multi-stable with an infinite number of wells. Numerous discrete models, directly aimed at the simulation of metal plasticity, are available in the literature ([20],[33],[34],[19],[18],[25],[12],[24]).

Several potential augmentations of the present model are worth mentioning. First, our assumption that the Maxwell force is the same for all elements generates over-symmetric "centered" inner loops, which should be considered only as a special feature of the present modification of the model. An introduction of the hard instead of the soft device will also bring new effects such as "saw-tooth" instead of "staircase" type serrations on the stress-strain curves. Adding to the picture interactions beyond nearest neighbors would allow one to mimic at least some of the non-one-dimensional features. Larger difficulties may be associated with the introduction of the under-damped, inertial dynamics. Finally, important and still unresolved issues are

associated with the construction of the adequate homogenized model reproducing the behavior of this and related systems in the continuum limit.

Acknowledgements. This work was supported by the research project Cofin-MURST2000 "Mathematical Models for Material Science" and by "Fondi di Ricerca di Ateneo" (GP), and by the NSF grant DMS-9803572 (LT).

Appendix I: Minimum barrier paths

Below we show that the minimum barrier path leaving the basin of a metastable state A (3.3) necessarily goes through the saddle S represented by a configuration identical to A in all respects except that the "softest" spring in phase I (with $i = \hat{k}$) is shifted to phase II (spinodal region). We assume for determinacy that $0 < \tilde{\sigma} < 1 - t_{\hat{k}}$; the case $t_{\hat{k}} - 1 < \tilde{\sigma} < 0$ can be treated similarly.

First observe that for $\tilde{\sigma} > 0$ the potential energy $\bar{G}$ of a metastable state grows with the number $\hat{k}$ of springs in phase I. Therefore, since we only consider paths going from A towards a metastable state with lower energy, we can assume that the $n - \hat{k}$ springs which are already in phase III do not switch wells. For instance, in the case of two springs studied in Sect. 3.1 this leads to the exclusion for $\tilde{\sigma} > 0$ of the path that goes from m_b $(1, 0, 1)$ to m_d $(2, 0, 0)$ (see Fig. 5d,f).

Consider now the neighborhood $\mathscr{N}$ of the minimum A

$$\mathscr{N} := \{\{\varepsilon_i\}_{i=1,\dots,n} \in \mathbf{R}^n : \varepsilon_i \le \varepsilon_i^{\mathrm{II}}, i \le \hat{k}; \varepsilon_i > t_i, i > \hat{k}\}. \tag{I.1}$$

Observe that $A \in \mathring{\mathscr{N}}$ and $S \in \partial\mathscr{N}$. The neighborhood $\mathscr{N}$ is constructed in such a way that any equilibrium state located strictly inside it must have all springs with $i \le \hat{k}$ in phase I and all springs with $i > \hat{k}$ in phase III. Thus the only critical point inside $\mathscr{N}$ is A. Now, to find the optimal "escape route", we minimize the energy on $\partial\mathscr{N}$. By using the assumption that the springs which are already in phase III do not switch back, we can limit our analysis to the edges of $\partial\mathscr{N}$ with $\varepsilon_i = \varepsilon_i^{II}$, $i \le \hat{k}$. The problem is to show that along these edges the minimum energy is attained at the saddle S.

Consider a generic ($n - l$ dimensional) edge corresponding to a configuration with $l \ge 1$ springs in phase II ($\varepsilon_h = \varepsilon_h^{II}$, $h \le \hat{k}$). The minimization of the potential energy G leads to the following Euler-Lagrange equations

$$\varphi_i'(\varepsilon_i) = \bar{\sigma}, \quad i = 1, \dots, n. \tag{I.2}$$

A solution C of (I.2) satisfies $C \in \partial\mathscr{N}$ only if $\varepsilon_i \in \{\varepsilon^I, \varepsilon^{II}\}, i \le \hat{k}$, and $\varepsilon_i = \varepsilon^{III}, i > \hat{k}$. Now we need to minimize among all these saddle-point solutions. To simplify the subsequent reasoning we introduce the potential energy of the i-th spring, $g_i(\varepsilon_i) := a(\varphi_i(\varepsilon_i) - \bar{\sigma}\varepsilon_i)$ and, using (1.2) and (2.2), compute

$$g_i(\varepsilon^I) = g^I := -a\left(\frac{\tilde{\sigma}^2}{2} - \tilde{\sigma}\right), \quad g_i(\varepsilon^{II}) = \frac{a}{2}\left(-\frac{t_i}{t_i - 1}\tilde{\sigma}^2 + 1 - t_i\right), \quad g_i(\varepsilon^{III}) = g^{III} := -a\left(\frac{\tilde{\sigma}^2}{2} + \tilde{\sigma}\right).$$

Since $t_i < t_{i+1}$, $i = 1, \dots, \hat{k} - 1$, for $0 < \tilde{\sigma} < 1 - t_{\hat{k}}$, we obtain the following ordering $g_1^{II} > \dots > g_{\hat{k}}^{II} > g^I > g^{III}$. By using this ordering it is now straightforward to show that the lowest energy is attained exactly at the saddle point configuration S with only one spring (the $\hat{k}$-th) in the spinodal state.

Appendix II: Return point memory and congruency properties

Return point memory property: *The parameters of the chain exhibit closed-loop trajectories under the following loading histories:*

$$\begin{aligned} &(a) \qquad s^h \to s_h \to s^{h+1} = s^h, \qquad |s_h| < |s^h|, \\ &(b) \qquad s_h \to s^{h+1} \to s_{h+1} = s_h, \qquad |s^{h+1}| < |s_h|. \end{aligned} \tag{II.1}$$

Consider the case (a). Notice that if $s_h > -\tilde{\sigma}_n$ no spring changes phase during the cycle and the system follows an elastic branch. Assume that $s_h \le -\tilde{\sigma}_n$, according to (a) we also have $s^h \ge \tilde{\sigma}_n$. Denote by i^h the

index of the spring satisfying $s^h \in [\tilde{\sigma}_{i^h}, \tilde{\sigma}_{i^h+1}[$. Then by using (4.8) we obtain that at $\tilde{\sigma} = s^h$ all springs with $\tilde{\sigma}_i \leq s^h$, *i.e.* the springs with $i \geq i^h$ must be in phase *III*. The initial state can then be characterized by

$$\chi_i^I(s^h) = \begin{cases} 0, & i \geq i^h, \\ \chi_i^I(s_{h-1}), & i < i^h. \end{cases} \tag{II.2}$$

Now if we denote by i_h the index of the spring satisfying $|s_h| \in [\tilde{\sigma}_{i_h}, \tilde{\sigma}_{i_h+1}[$, we obtain that at $\tilde{\sigma} = s^{h+1} = s_h$ all springs with $i \geq i_h$ must switch back to phase *I*, producing an equilibrium configuration with

$$\chi_i^I(s_h) = \begin{cases} 1, & i \geq i_h, \\ 0, & i^h \leq i < i_h, \\ \chi_i^I(s_{h-1}) & i < i^h. \end{cases}$$

Finally at $\tilde{\sigma} = s^{h+1} = s^h$ all springs with $i \geq i^h$ must switch back to phase *III*, and we again obtain our initial state (II.2). The case (*b*) is analogous.

Congruency property: *The loading paths (II.1) generate congruent loops independently of the initial configuration.*

Consider again the case (*a*) and suppose that the index i^h has the same meaning as above. By the time the load reaches the value $\tilde{\sigma} = s^h$ all springs with $i \geq i^h$, independently of the initial conditions, must be in phase *III*. When the load is decreasing the system exhibits an elastic unloading following metastable branches with the same slope $E = 1$ (see 2.5). At $\tilde{\sigma} = -\tilde{\sigma}_n$ the n-th spring which is in phase *III* undergoes a transition to phase *I* leading to the strain discontinuity $[\![\varepsilon]\!] = -2/n$. Afterwards both systems follow the same sequence of elastic steps interrupted by the same strain discontinuities at the transition loads (4.8) as the springs with $i \geq i_h \geq i^h$ switch back to phase *I*. Similarly, congruent paths are followed when the load is increasing and the springs with $i \geq i_h$ transform back to phase *III*. The result can be easily extended to the case (b).

References

1. Abeyaratne R, Chu C, James RD (1996) Kinetics of materials with wiggly energies: theory and applications to the evolution of twinning microstructures in a Cu-Al-Ni shape memory alloy. Phil. Mag. A 73(2): 457–497
2. Balk AM, Cherkaev AV, Slepyan LI (20019 Dynamics of solids with non-monotone stress-strain relations. 1. Model and numerical experiments. J. Mech. Phys. Sol. 49(1): 131–148
3. Balk AM, Cherkaev AV, Slepyan LI (2001) Dynamics of solids with non-monotone stress-strain relations. 2. Nonlinear waves and waves of phase transition. J. Mech. Phys. Sol. 49(1): 149–171
4. Bell JF (1973) The Experimental Foundations of Solid Mechanics. Handbuch der Physic VIa/1. Springer, Berlin
5. Bertotti G (1999) Hysteresis in magnetism. Academic Press
6. Cardin F, Favretti M (2001) Dynamics of a chain of springs with non convex potential energy. Preprint n. 6 Dipartimento di Matematica Pura e applicata, Univ. di Padova
7. Chaboche JL, Nouailhas D, Paulmier P, Policella H (1989) Sur les problèmes posés par la description des effets de rochet en plasticité et viscoplasticité cycliques. La Recerque Aérospatiale 1: 63–79
8. Christian JW, Mahajan S (1995) Deformation twinning. Prog. Mat. Sci. 39: 1–157
9. Dutkiewicz J, Kato H, Miura S, Messerschmidt U, Bartsch M (1996) Structure changes during pseudoelastic deformation of CuAlMn single crystals. Acta Mater. 44(11): 4597–4609
10. Fedelich B, Zanzotto G (1992) Hysteresis in discrete systems of possibly interacting elements with a double-well energy. J. Nonlinear Sci. 2: 319–342
11. Frenkel YI, Kontorova TI (1938) Zh. Eksp. Teor. Fiz. 8: 1340
12. Froli M, Royer-Carfagni G (2000) A mechanical model for the elastic-plastic behavior of metallic bars. Int. J. Sol. Str. 37: 3901–3918
13. Maher VM, Crone WC, Shield TW (1999) Displacement history effect on the pseudoelastic behavior of shape-memory wires. Preprint
14. Mayergoyz ID (1991) Mathematical models of hysteresis. Springer, New York
15. Müller I (1985) Pseudoelasticity in Shape Memory Alloys – An Extreme Case of Thermoelasticity, volume 168 of Reports of IMA
16. Müller I, Seelecke S (1996) Thermodynamics Aspects of Shape Memory Alloys. Reports of the Technical University of Berlin
17. Müller I, Villaggio P (1977) A model for an elastoplastic body. Arch. Rat. Mech. Anal. 65: 25–46
18. Mroz Z (1967) On the description of anisotropic work hardening. J. Mech. Phys. Sol. 15: 163–175
19. Nabarro FRN (1987) Theory of Crystal Dislocations. Dover, New York
20. Nadai A (1950) Theory of Flow and Fracture of Solids. McGraw-Hill, New York
21. Nishimura F, Watanabe N, Tanaka K (1987) Evolution of martensite start condition in general thermomechanical loads of Fe-based shape memory alloys. Acta Metal. 35(11): 2779–2789

22. Ortin J (1992) Preisach modeling of hysteresis for a pseudoelastic Cu-Zn-Al single crystal. J. Appl. Phys. 71(3): 1454–1461
23. Pattor E, Eberhardt A, Berveiller M (1987) Potentiel pseudoélastique et plasticité de transformation martensitique dans les mono et polycristaux métalliques. Acta Metal. 35(11): 2779–2789
24. Ponter ARS, Bataille J, Kestin J (1979) A thermodynamical model for the time dependent plastic deformation of solids. J. Mécanique, pp 511–539
25. Prager W (1955) The theory of plasticity. A survey of recent achievements. Proc. Inst. Mech. Eng., (London) (169): 41–57
26. Puglisi G, Truskinovsky L (2000) Mechanics of a discrete chain with bi-stable elements. J. Mech. Phys. Sol. 1: 1–27
27. Puglisi G, Truskinovsky L (2001) Rate independent hysteresis in a bi-stable chain. J. Mech. Phys. Sol. 50(2): 165–187
28. Rogers R, Truskinovsky L (1997) Discretization and hysteresis. Physica B 233(4): 370–375
29. Rosakis P, Rosakis AJ, Ravichandran G, Hodowany J (2000) A thermodynamic internal variable model for the partition of the plastic work into heat and stored energy in metals. J. Mech. Phys. Sol. 48(3): 581–607
30. Slepyan LI (2001) Feeding and dissipative waves in fracture and phase transition. I Some 1D structures and a square-cell lattice. J. Mech. Phys. Sol. 49: 469–511
31. Slepyan LI (2001) Feeding and dissipative waves in fracture and phase transition. II Phase transition waves. J. Mech. Phys. Sol. 49: 513–550
32. Slepyan LI, Troiankina LV (1988) Fracture wave in a chain structure. J. Appl. Mech. Tech. Phys. 25: 921–927
33. Taylor GI (1934) The mechanism of plastic deformation, part I, theoretical. Proc. Roy. Soc. London A 145: 362–387
34. Taylor GI (1934) The mechanism of plastic deormation, part II, comparison with oxbervations. Proc. Roy. Soc. London A 145: 388–404
35. Tóth LS, Molinari A, Zouhal N (2000) Cyclic plasticity phenomena as predicted by polycrystal plasticity. Mech. Mat. 32: 99–113
36. Truskinovsky L (1996) Fracture as Phase Transformation, pp 322–332. In: Batra RC, Betty MF (eds) Contemporary research in the mechanics and mathematics of materials, CIMNE. Barcelona
37. Zaiser M, Hähner P (1997) Oscillatory modes of plastic deformation: Theoretical concepts. Phys. Stat. Sol. (b) 199: 267–330